Comprehensive cell biological investigation of cytochalasin B derivatives with distinct activities on the actin network.

Mervic D. Kagho,[‡,1] Katharina Schmidt,[‡,2] Christopher Lambert,[2,3,4] Thomas Kaufmann,[5] Lili Jia,[3] Jan Faix,[5] Klemens Rottner,[2,4] Marc Stadler,[3] Theresia Stradal,[*,2] and Philipp Klahn[*,1]

[1]Department of Chemistry and Molecular Biology, Division of Medicinal Chemistry, University of Gothenburg, Medicinaregatan 7B, SE-413 90 Göteborg, Sweden.

[2]Department of Cell Biology, Helmholtz Centre for Infection Research, Inhoffenstrasse 7, D-38124 Braunschweig, Germany.

[3]Department of Microbial Drugs, Helmholtz Centre for Infection Research, Inhoffenstrasse 7, D-38124 Braunschweig, Germany.

[4]Division of Molecular Cell Biology, Zoological Institute, Technische Universität Braunschweig, Spielmannstrasse 7, D-38106 Braunschweig, Germany.

[5]Institute for Biophysical Chemistry, Hannover Medical School, Carl-Neuberg Strasse 1, D-30625 Hannover, Germany.

ABSTRACT: In search of a more comprehensive structure activity relationship (SAR) regarding the inhibitory effect of cytochalasin B (**CB**) on actin polymerization, a virtual docking of **CB** onto monomeric actin was conducted. This led to the identification of potentially important functional groups of **CB** (i.e. the NH group of the isoindolone core (N-2), and the hydroxyl groups at C-7 and C-20) involved in interactions with the residual amino acids of the binding pocket of actin. Chemical modifications of **CB** at positions C-7, N-2, and C-20 led to derivatives **CB1**-**CB4**, which were analyzed for their bioactivities. **CB1**-**CB4** exhibited reduced or no cytotoxicity in murine L929 fibroblasts compared to **CB**. Moreover, short- and long-term treatments of human osteosarcoma cells (U-2OS) affected the actin network to variable extent, partially accompanied by the induction of multinucleation. Derivatives displaying acetylation at C-20 and N-2 were subject to slow intracellular conversion to highly cytotoxic **CB**. Together, this study highlights the importance of the hydroxy group at C-7 and the NH function at N-2 for **CB** potency on the inhibition of actin polymerization.

Cytochalasans are fungal secondary metabolites found in many genera across the Ascomycota with the largest proportion of compounds described for *Diaporthe* and *Chaetomium*. Cytochalasans are biosynthesized by fungal polyketide synthetase – non-ribosomal peptide synthetases (PKS-NRPS) through fusion of a polyketide chain with an amino acid-derived building block.[1] The resulting acyclic precursor undergoes a crucial late-stage *Diels-Alder* (DA) cyclization forming the tricyclic core structure of the cytochalasan natural product family, which is further modified during the biosynthesis by oxidative rearrangements and cationic cyclizations contributing to the huge structural diversity of these compounds.[2] Cytochalasans display a broad spectrum of bioactivities and were ascribed antimicrobial, antiparasitic, or antiviral activities.[3] The most prominent activity of cytochalasans however is the disruption of the actin cytoskeleton, resulting in impairment of cell shape and behavior.[4]

Actin plays a crucial role in most if not all motile processes of eukaryotic cells, including changes of cell shape, cell migration, vesicular trafficking, and cytokinesis.[5] Actin undergoes dynamic cycles of polymerization and depolymerization. Biochemically, above the so-called critical concentration, monomeric globular actin (G-actin) spontaneously polymerizes into filamentous actin (F-actin) polymers, with preferred addition to one end termed the fast growing (also plus or barbed) end. The other end, termed the minus (or pointed) end, displays a higher critical concentration, causing a reduced polymerization rate as compared to the barbed end. At monomer concentrations in between the critical concentration at the two ends, the barbed and pointed ends thus display polymerization and depolymerization, respectively.[6] In cells, actin filaments organize into various structures mediated by multiple actin filament binding proteins. This brings about a variety of actin architectures, such as branched filament networks (e.g. found in lamellipodia or vesicular structures), parallel filament bundles (as found in filopodia), or anti-parallel bundles (as in stress fibers). Actin filament binding factors display multiple activities, not only including parallel or anti-parallel bundling, but also capping of filament ends, filament severing or even their crosslinking and branching. Actin monomers are tightly regulated as well, for instance by profilin, which aids monomer addition onto filament barbed ends but also blocks their spontaneous nucleation, whereas the latter is spatially and temporally controlled by distinct classes of nucleators or nucleation promoting factors.[7]

According to the most widely accepted model of actin-cytochalasin interaction, members of this compound family bind actin filament barbed ends, thought to inhibit the addition of new monomers.[8]

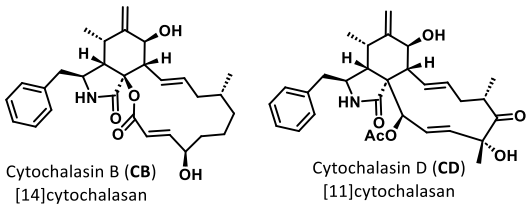

Figure 1 Structures of cytochalasin B (**CB**) and cytochalasin D (**CD**)

Due to the interference with actin polymerization, cytochalasin-treated cells display compromised, actin assembly-dependent structures, coinciding with a high cytotoxicity in cultured cell lines of these compounds ranging from sub-micromolar to nanomolar concentrations.[9] Hence, successful clinical application would require balancing projected toxicity and therapeutic benefit. This goal will require an in depth understanding of how distinct chemical moieties affect the activity of a given cytochalasan. A variety of structure activity relationship (SAR) studies have been published over the past decades,[4] attempting to shed light on the complexity of cytochalasan activity and diversity. Conclusions drawn from previous SAR studies include a pivotal role of the C-7 hydroxy group, while the amino acid incorporated in the isoindolone core will likely not affect activity.

Notably, *bona-fide*, detailed structural information on the interaction of cytochalasans with the actin filament barbed end is currently missing. The best approximation of this interaction derived from a co-crystal of a non-polymerizable actin variant in complex with cytochalasin D (**CD**, Figure 1), published in 2008.[10] The orientation of **CD** in the binding pocket is strongly guided by polar contact and hydrophobic interactions at the back half of the hydrophobic cleft (compare Figure 2A). However, a comprehensive SAR of other cytochalasans on actin remains a challenging task. For instance, the precise mode of binding of cytochalasin B (**CB**, Figure 1), the second among the most frequently employed cytochalasans, to actin remains unknown. For this reason, we conducted a molecular docking of **CB** onto the previously described, non-polymerizable actin variant,[11] to predict functional groups of this molecule potentially mediating its interaction with actin. We then tested derived hypotheses by semi-synthetically modifying these functional groups of **CB,** e.g. by acetylation and methylation, with the aim to generate derivatives with potentially altered activities on F-actin organization in cells or cytotoxicity. We thus obtained a precise determination of those positions in the **CB** backbone relevant for its bioactivities, using both cell biological and *in vitro* actin polymerization assays.

RESULTS AND DISCUSSION

Virtual docking of CB onto monomeric actin. In order to understand the mode of binding of **CB** to actin, we generated 724 conformers of an energy-minimized structure of **CB** using the conformer ensemble generator Conformator.[12] A virtual docking of these conformers into the binding pocket of **CD** on monomeric G-actin (PDB: 3EKU)[10] obtained in 2008 by *Nair et al.* was performed and compared to **CD**. The utilized co-crystal structure of **CD**[10] is based on a non-polymerizable actin mutant from *Drosophila melanogaster* bearing two point mutations (A204E/P243K), referred to as AP-actin,[11] which is thought to retain all biochemical and structural characteristics compared to tissue-purified G-actin.[13] It needs to be mentioned that cytochalasans such as **CB** and **CD** are known to bind the barbed end of F-actin and not to usually interact with G-actin except for the non-polymerizable AP-actin mutant. Very recently, two cryo-EM structures of the barbed end of F-actin have been reported.[14,15] However, since our approaches to dock **CD** or **CB** onto these structures have so far not yet yielded reasonable results, we decided to proceed with AP-actin for our own docking studies. As described earlier by Nair et al.,[10] **CD** binds this actin variant displaying a distinct network of six intramolecular hydrogen bonding interactions with the actin backbone as outlined in Figure 2A. Five of these are mediated by the functional groups in the isoindolone core of **CD**. Two hydrogen bonds are formed between the amide NH at N-2[16] oriented deep into the binding pocket with Tyrosine-143 (Tyr143) and Glycine-168 (Gly168). Furthermore, the oxo group of **CD** at the C-1 position of the isoindolone core serves as hydrogen bond acceptor for the NH at Alanine-170 (Ala170). In addition, the hydroxy group at C-7 position of the isoindolone core, which points deep into the binding pocket as well, is involved in two hydrogen bonds. One as hydrogen bond acceptor for the NH at Isoleucin-136 (Ile136), and the other as hydrogen bond donor towards a molecule of water, which is positioned within a local network of hydrogen bonds between Valine-134 (Val134) and Cystein-374 (Cys374) of the actin backbone. Finally, one hydrogen bond occurs between the hydroxy group at C-8 of the 11-membered macrocycle of **CD** and the oxo moiety of Alanine-170 (Ala170). An additional intramolecular hydrogen bond with the C-17 oxo group of **CD** further stabilizes the overall complex.

Our docking of **CB** into the same binding pocket resulted in an overall similar mode of binding compared to **CD** as outlined in Figures 2B and 2C. However, the more sterically demanding 14-membered macrocycle seemed to not allow **CB** to penetrate as deeply into the pocket compared to **CD** and furthermore shifted the overall position of **CB** in the binding pocket by roughly 1.51-1.78 Å with huge impact on the hydrogen bond network. In comparison to **CD**, the NH group at N-2 position and the oxygen atom of the oxo group at C-1 of the isoindolone core of **CB** are lifted out of the pocket by 1.37 Å and 1.92 Å, respectively (Figure 2C). The larger distance to Ala170 and Tyr143 prevents the formation of two hydrogen bonds as seen for **CD** (Compare Figure 2B and A). Furthermore, the hydroxyl group at C-7 of the isoindolone core of **CB** is shifted by 1.78 Å away from the NH of the Ile136 (Figure 2C) preventing the formation of a hydrogen bond as seen for **CD** (Compare Figure 2B and A). Overall, the docking suggested a significantly reduced estimated binding affinity of **CB** for actin compared to **CD**, in line with the observed diminished bioactivity if comparing **CD** and **CB**.[17]

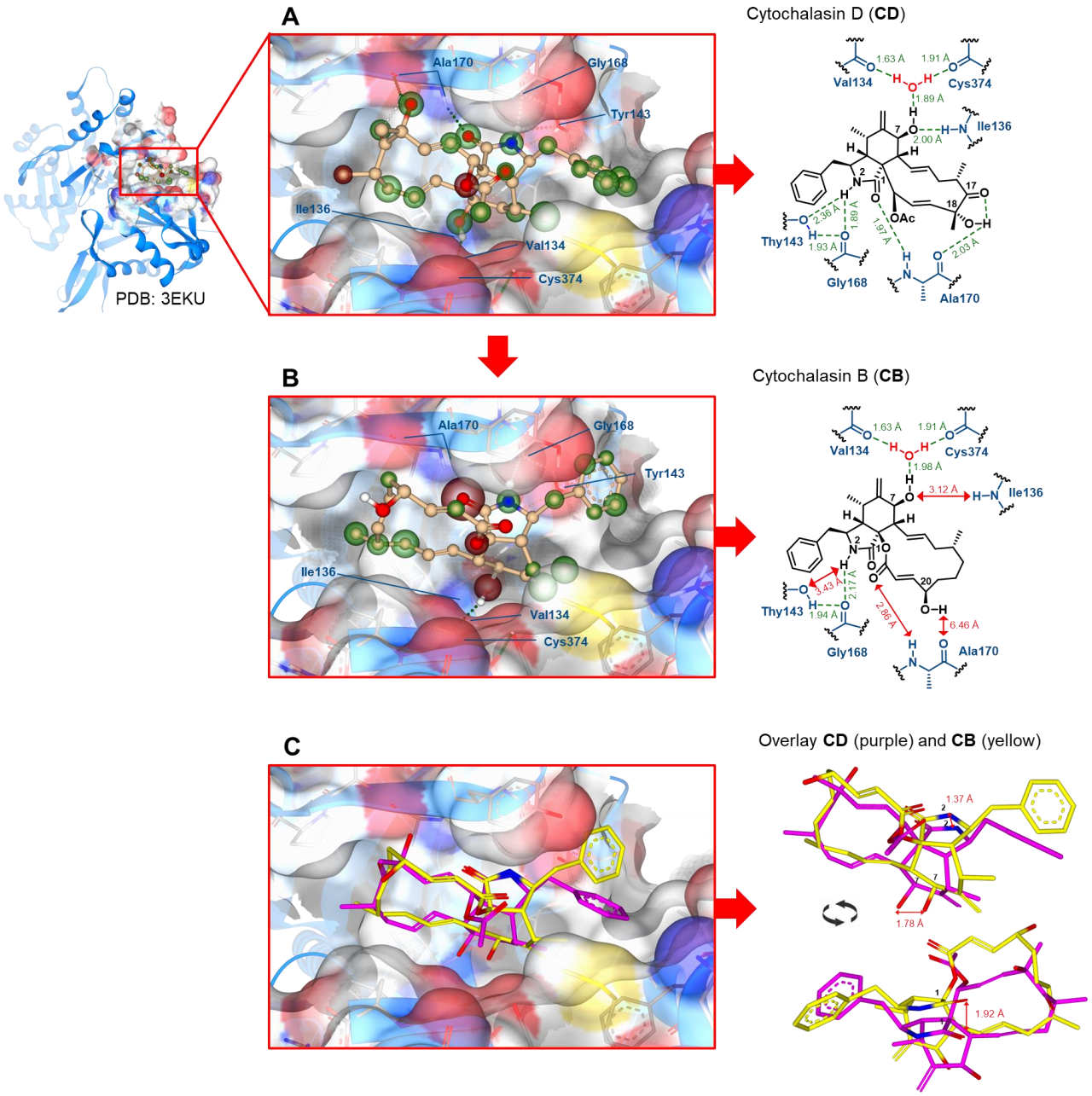

Figure 2. Docking of **CB** onto monomeric actin: (A) 3D illustration of the co-crystal structure (PDB:3EKU)[10] of non-polymerizable monomeric actin and cytochalasin D (**CD**) with main hydrogen bridge network; (B) 3D illustration of the docking of **CB** into the binding pocket of **CD** on monomeric actin (PDB:3EKU)[10]; (C) 3D illustration of the overlay of **CD** (purple) and **CB** (yellow) within the binding pocket on monomeric actin. Docking was performed and 3D-illustration were generated with SeeSAR version 13.0.5; BioSolveIT GmbH, Sankt Augustin, Germany, 2023, www.biosolveit.de/SeeSAR.[18] Green spheres around atoms indicate overall favourable contributions to $\Delta G_{(Hyde)}$, red spheres around atoms indicate overall unfavourable contributions to $\Delta G_{(Hyde)}$.[19] Hydrogen bridges are indicated by dotted green lines with distances between hydrogen atoms and donor heteroatom given in Å in green. General distances between atoms are given in Å in red. Light grey illustration represents surface of the binding pocket with elements surrounding the bound cytochalasans in red (oxygen), blue (nitrogen) and yellow (sulfur). Grey shadows represent unoccupied space in the binding pocket. Numbering of atoms in cytochalasans follows the nomenclature applied by *Binder et al.*[20]

Based on this docking, we estimated that the amide NH group at N-2, and the hydroxy function at C-7 will be vital for the activity of **CB** on actin, while the hydroxy function at C-20 appeared to be less involved in binding.

Semi-synthetic derivatization of CB. To biologically validate the importance of these moieties for the overall actin binding and cytotoxic activity of **CB**, we semi-synthetically modified **CB** at the N-2 NH as well as the C-7 and C-20 hydroxy functions by methylation and acetylation as outlined in Scheme 1 obtaining the derivatives 7-*O*-acetyl

cytochalasin B (**CB1**), *N*-methyl cytochalasin B (**CB2**), *N*-acetyl cytochalasin B (**CB3**) and 20-*O*-acetyl cytochalasin B (**CB4**).

7-*O*-Acetyl cytochalasin B (**CB1**) was obtained via two different routes. In the first route, selective *O*-silylation of the C-20 hydroxy function occurred, when **CB** was treated with TBSCl in the presence of imidazole and sub-stochiometric amounts of DMAP at 40°C, yielding compound **1** in 80 % yield. Subsequent reaction with a three-fold excess of acetic anhydride in the presence of triethylamine and stoichiometric amounts of DMAP led to the formation of 7-acetyl derivative **2** in 92 % yield. Finally, treatment with a mixture of HF:TBAF/3:1[21] afforded **CB1** in 70 % yield and 81 % overall yield from **CB**. In a second route, double acetylation towards 7,20-*O,O'*-diacetyl cytochalasin B (**3**) was achieved in the presence of a five-fold excess of acetyl chloride with triethylamine and stoichiometric amounts of DMAP in 98 % yield. Afterwards, treatment of **3** with 1.2 equivalents of K_2CO_3 in anhydrous methanol led to selective acetyl cleavage at C-20 position, yielding **CB1** with 97 % (Scheme 1).

The deshielding of the proton at C-7 from 3.80 ppm (d, 1H) in the parental **CB** to 5.28 ppm (d, 1H) in **CB1** in the ^{1}H-NMR spectra clearly indicated the *O*-acetylation of the C-7 hydroxyl group, while the signal for the proton at the C-20 position remained at around 4.46–4.51 ppm (m, 1H). Additionally, heteronuclear multiple bond correlation (HMBC) long-range ^4J-coupling between the proton at C-7 and the carbonyl carbon of the introduced acetyl group (5.28 ppm/170.09 ppm, see Figure S17 in the Supplementary Information) provided further analytical evidence for *O*-acetylation of the hydroxyl function at C-7.

Interestingly, reaction of **CB** in the presence of five equivalents of sodium hydride in dry DMF and subsequent treatment with an excess of methyl iodide did not lead to formation of *O*-methylated cytochalasin B derivatives, but instead gave rather selective access to *N*-methyl cytochalasin B (**CB2**) in 80 % yield.

The successful *N*-methylation at position N-2 was proven by the presence of a singlet with an integral corresponding to 3 hydrogen atoms at 2.83 ppm in the ^{1}H-NMR spectrum of **CB2** (see Figure S20 in the Supplementary information) and the respective *N*-methyl carbon in the ^{13}C-NMR spectrum of **CB2** at 28.52 ppm, exhibiting a heteronuclear multiple bond correlation (HMBC) long-range ^4J-coupling with the methylene protons at C-10 (2.74 ppm) (see Figure S21 in the Supplementary Information). The *N*-acetylation of **CB** towards *N*-acetyl cytochalasin B (**CB3**, Scheme 1) was achieved in three steps. First, conversion of **CB** in the presence of a 10-fold excess of TBSCl, imidazole and stoichiometric amounts of DMAP at 40°C gave access to the double *O*-silylated intermediate **4** in 85 % yield. Reaction of **4** with sodium hydride in anhydrous DMF and subsequent treatment with acetyl chloride furnished *N*-acetylation towards compound **5**. Final TBS deprotection with TBAF gave *N*-acetyl cytochalasin B (**CB3**) in 50 % yield along with some **CB** indicating the lability of the *N*-acetyl function towards basic conditions.

Finally, the reaction of **CB** with acetic acid anhydride in the presence of triethyl amine led to the selective formation of 20-*O*-acetyl cytochalasin B (**CB4**) in 70% yield (Scheme 1). **CB4** was distinguishable from **CB1** by TLC (hexane:EtOAc/1:1), R_f(**CB1**): 0.50, and R_f(**CB4**): 0.47 [UV^{254}, CAM].

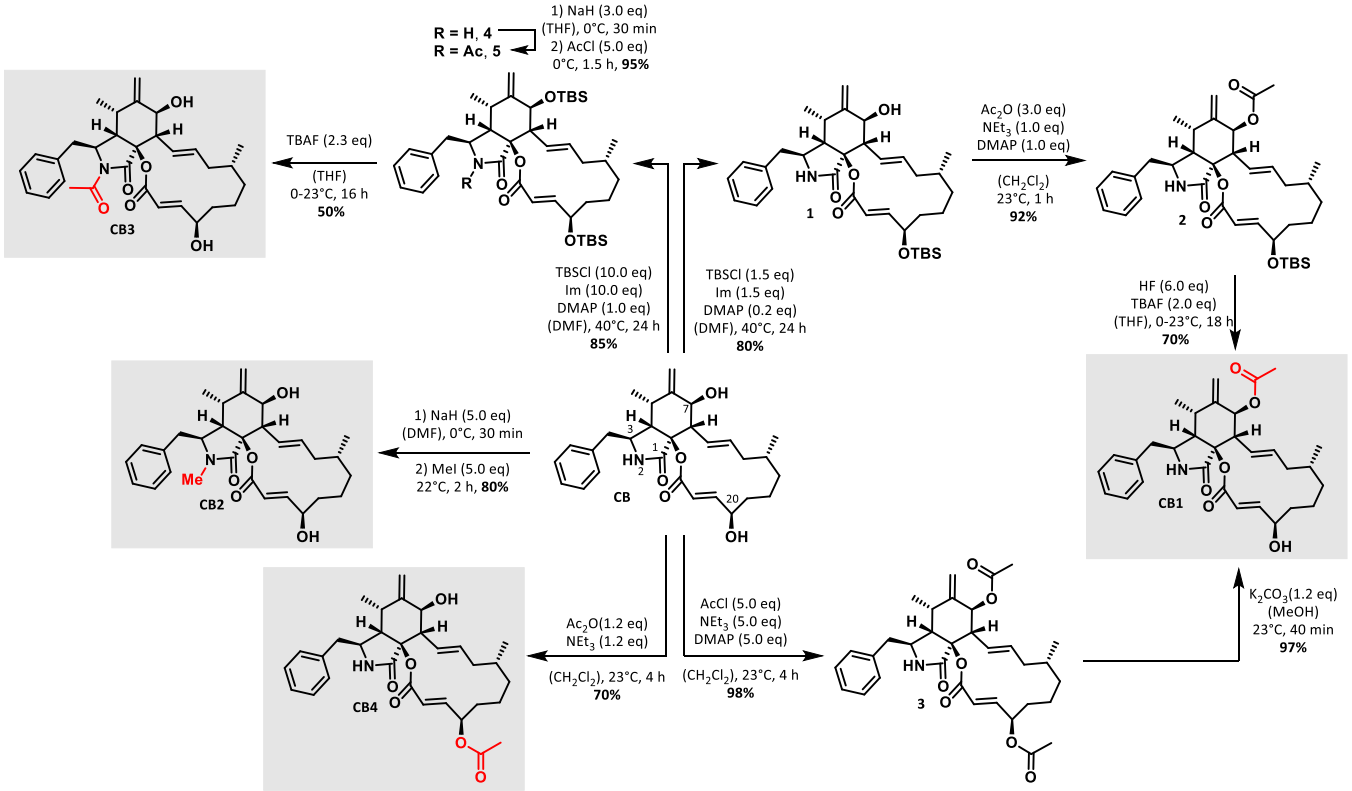

Scheme 1 Semi-synthetic modification of **CB** towards 7-*O*-acetyl cytochalasin B (**CB1**), *N*-methyl cytochalasin B (**CB2**), *N*-acetyl cytochalasin B (**CB3**) and 20-*O*-acetyl cytochalasin B (**CB4**).

Furthermore, the deshielding of C-20 proton (5.49-5.52 ppm, m, 1H)) compared to the C-7 OH proton (3.88 ppm, d, 1H) was taken as proof for *O*-acetylation of the hydroxy function at C-20. Additionally, further analytical evidence for *O*-acetylation of the hydroxyl function at C-20 was provided by a heteronuclear multiple bond correlation (HMBC) long-range ^{4}J-coupling between the proton at C-20 and the methyl carbon of the introduced acetyl group (5.51 (5.49-5.52) ppm/20.97 ppm, see Figure S34 in the Supplementary Information). With the derivatives **CB1** – **CB4** in hand, we next conducted a comprehensive biological evaluation of the compounds to elucidate the impact of the modifications on their efficacy against actin and their overall cytotoxicity.

Biological evaluation of CB derivatives. First, the antimicrobial effects of compounds **CB1**, **CB2**, **CB3**, and **CB4** against a variety of bacteria and fungi were examined. These included *Staphylococcus aureus*, *Bacillus subtilis*, *Mycobacterium smegmatis*, *Escherichia coli*, *Pseudomonas aeruginosa*, *Chromobacterium violaceum*, *Acinetobacter baumannii, Schizosaccharomyces pombe, Pichia anomala, Mucor hiemalis, Candida albicans,* and *Rhodotorula glutinis*. **CB1** exhibited weak antibacterial activity against *Mycobacterium smegmatis* with a minimum inhibitory concentration (MIC) of 66.6 µg/mL. In addition, **CB4** showed a moderate MIC with 33.3 µg/mL against *Schizosaccharomyces pombe.* All other substances had no antibacterial or antifungal activity against any of the tested microorganisms.

Second, **CB** and its four derivatives **CB1**, **CB2**, **CB3**, and **CB4** were evaluated for their cytotoxic effects in two tumor cell lines, namely mouse connective tissue fibroblasts L929 and human cervix carcinoma cells KB3.1 (Table 1). Compared to their derivatives, **CB** showed cytotoxic effects in L929 with an IC_{50} value of 1.3 µM, whereas **CB1**, **CB3** and **CB4** exhibited clearly reduced but still moderate cytotoxicities ranging from 4.8 to 26.8 µM in both cell lines.

Table 1. Cytotoxicity of **CB**, **CB1**, **CB2**, **CB3**, and **CB4** tested against L929 and KB3.1 cell lines.[22,23]

	IC_{50} [µM]	
	L929	KB3.1
CB	1.3	n.t.
CB1	15.9	26.8
CB2	NC	85.0
CB3	9.4	7.9
CB4	4.8	n.t.
Epothilone B	$5.78 \pm 1.02 \times 10^{-4}$	$9.45 \pm 5.63 \times 10^{-5}$

NC: no cytotoxic effect, or only weak inhibition of proliferation; n.t.: not tested.

In contrast, **CB2** displayed very low or no cytotoxicity in KB3.1 (85 µM) and L929 cells, respectively, with weak antiproliferative activity in L929 (Table 1).From this, we concluded that the almost complete loss of cytotoxicity is caused by the incorporation of a methyl group at the N-2 position of the isoindolone core in **CB2**, whereas the *O*-acetylation at hydroxyl groups at C-7 and C-20 in derivatives **CB1** and **CB4** respectively, as well as the *N*-acetylation at N-2 position in **CB3** seemed to affect cytotoxicity less dramatically (Table 1).

A well-established *in cellulo* actin disruption assay was employed to study the effects of the derivatives **CB1**, **CB2**, **CB3**, and **CB4** as opposed to the known effect of **CB** on the F-actin network.[17] For this, the human osteosarcoma cell line U-2OS was treated using concentrations estimated based on previously determined IC_{50} values in murine L929 fibroblasts (Table 1), referred to as low dose (1 × IC_{50}), and a five-fold concentration, referred to as high dose (5 × IC_{50}). Reorganization of the F-actin network was also investigated upon high dose treatment followed by washout and a 1 h recovery phase in fresh medium. The impact on F-actin network organization was visualized using fluorescently labelled phalloidin (Figure 3). Cells treated with DMSO as vehicle control (Figure 3f, 3l and 3r) displayed distinct F-actin structures like lamellipodia – F-actin-rich meshworks at the cell periphery (green arrowheads) - and stress fibers - antiparallel, contractile F-actin bundles (red arrowheads). A low dose treatment of cells with **CB** and **CB4** led partially to compromised lamellipodia and a reduction of intermittent cytoplasmic F-actin (Figure 3a and e), whereas effects of the other derivatives were mostly indiscernible from the DMSO control (Figure 3b-d). Higher concentrations of **CB** and **CB4** caused a complete collapse of the F-actin network, manifesting in the formation of knot-like, F-actin rich accumulations (Figure 3g and k), whereas **CB2** and **CB3** induced only slight and **CB1** no such structures (Figure 3h-j). In addition, the effects on F-actin structures observed upon high dose treatment of all compounds were fully reversible after 1 h recovery time (Figure 3m-q).

In conclusion, a correlation between chemically modified positions in the backbone of **CB** and actin disruption activity was uncovered, as C-7 and N-2 modified derivatives showed reduced or no actin inhibition activity in this experimental set-up. Surprisingly, acetylation of the C-20 position as in **CB4** reduce cytotoxicity but preserved the activity on actin as observed for **CB**.

To rule out that the reduced *in cellulo* efficacies of **CB1**-**CB3** could instead be explained by an altered membrane permeability of modified compounds or their differential effects on other intracellular factors, pyrene actin polymerization assays[24] were used to analyze potential effects on actin assembly *in vitro* under defined conditions. Globular actin (G-actin) was purified from rabbit skeletal muscle[25] and fluorescently labeled with pyrene (see description in the Supplementary Information). 2 µM G-actin supplemented with 5% pyrene-labeled actin was added to actin seeds and respective compound (2 µM) in polymerization buffer to initiate the reaction.

Actin polymerization was then assessed by an increasing pyrene fluorescence signal over time (Figure 4). Equimolar amounts of **CB** (red) and **CB4** (brown) significantly reduced the polymerization rate of actin to 45 % and 58 %, respectively, compared to the DMSO control (green). In contrast, the derivatives **CB2** and **CB3** (purple, blue) by trend, but not in a statistically significant fashion inhibited polymerization (84-86%), while **CB1** (orange) had no effect or even slightly increased it (107%).

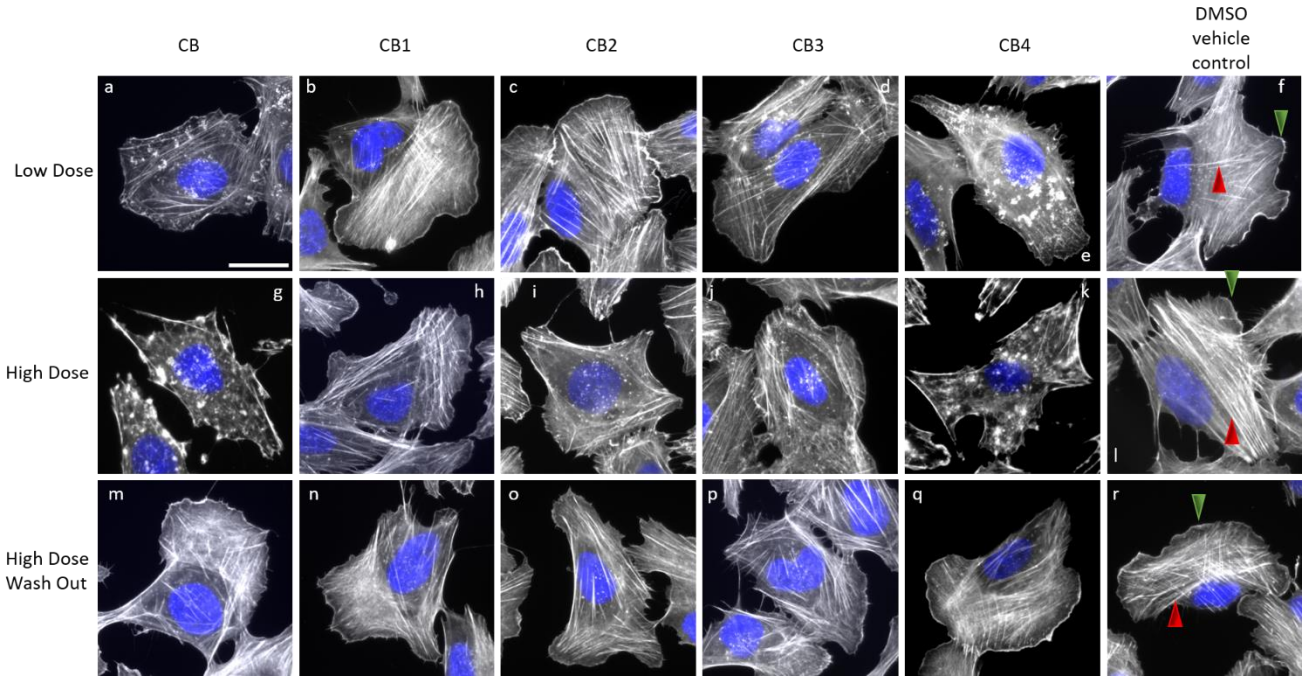

Figure 3. Overlay images of U-2OS wt cells treated with different concentrations of compounds **CB** (a, g), **CB1** (b, h), **CB2** (c, i), **CB3** (d, j), and **CB4** (e, k). Compound concentrations were based on previously determined IC_{50} values in L929 mouse fibroblast cells (low dose: 1 × IC_{50}, a-f; high dose: 5 × $IC_{50, g\text{-}l}$). DMSO (f, l, and r) was used as vehicle control, and a recovery experiment corresponded to high dose-treatment (as above) followed by 1 h recovery in full growth medium (high dose wash out, m-r). Cells were fixed with *para*formaldehyde and stained for their F-actin network using fluorescently labelled phalloidin (white) and their nuclear DNA using DAPI (*pseudo* coloured in blue). Described F-actin rich structures like lamellipodia (green arrowheads) and stress fibers (red arrowheads) are highlighted in (f, l, and r). The representative scale bar in (a) corresponds to 25 µm.

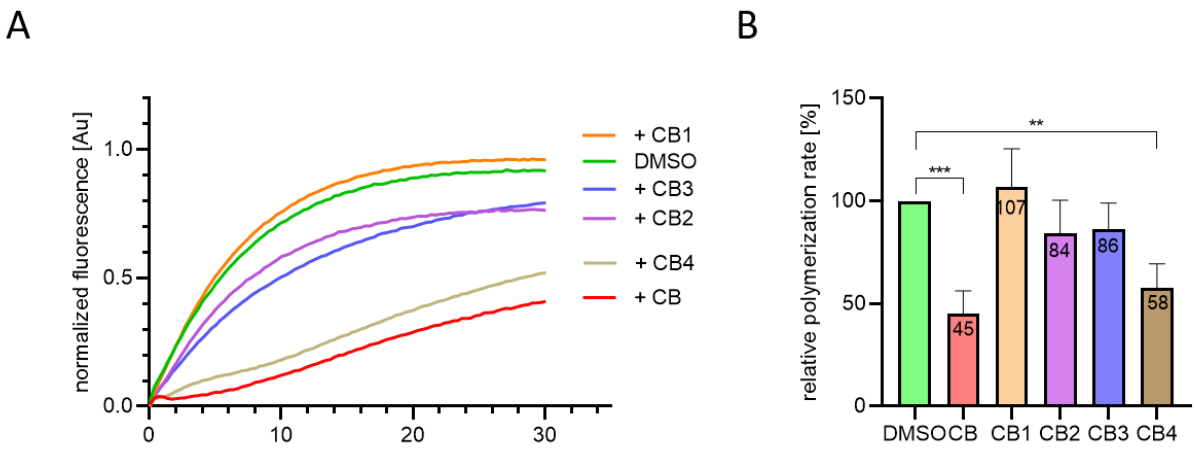

Figure 4 Effects of **CB** and derivatives on *in vitro* actin polymerization. (A) Pyrene assays were performed using 2 µM actin supplemented with 5% pyrene-actin. Polymerization was initiated by injecting G-actin into a solution containing actin polymerization buffer and 550 nM actin seeds. Normalized fluorescence intensities [Au] of actin polymerization curves were plotted over time. The graph shows the mean normalized fluorescence intensity from at least two independent experiments with 2 replicates each. (B) Relative actin polymerization rate [%] after 30 min. Data show means ± SD; n = 2. *** $p < 0.0002$, ** $p < 0.0015$, ordinary one-way ANOVA.

These results allowed us to exclude that reduced membrane permeability of the compounds is causative of the reduced activity *in cellulo*. Dynamic actin assembly in cells is crucial for many processes such as protrusion (e.g. of lamellipodia) or adhesion.[5] Thus, we next asked whether these compounds interfered with cell attachment. However, no differences were observed for the five compounds compared to DMSO (data not shown). Of note, however, the experiments revealed a significant reduction of cell size after 24 h treatment (data not shown).

To better understand these long-term effects, we extended the 1 h endpoint assay to 24 h high dose treatment and visualized the actin network as described above (Figure 5).

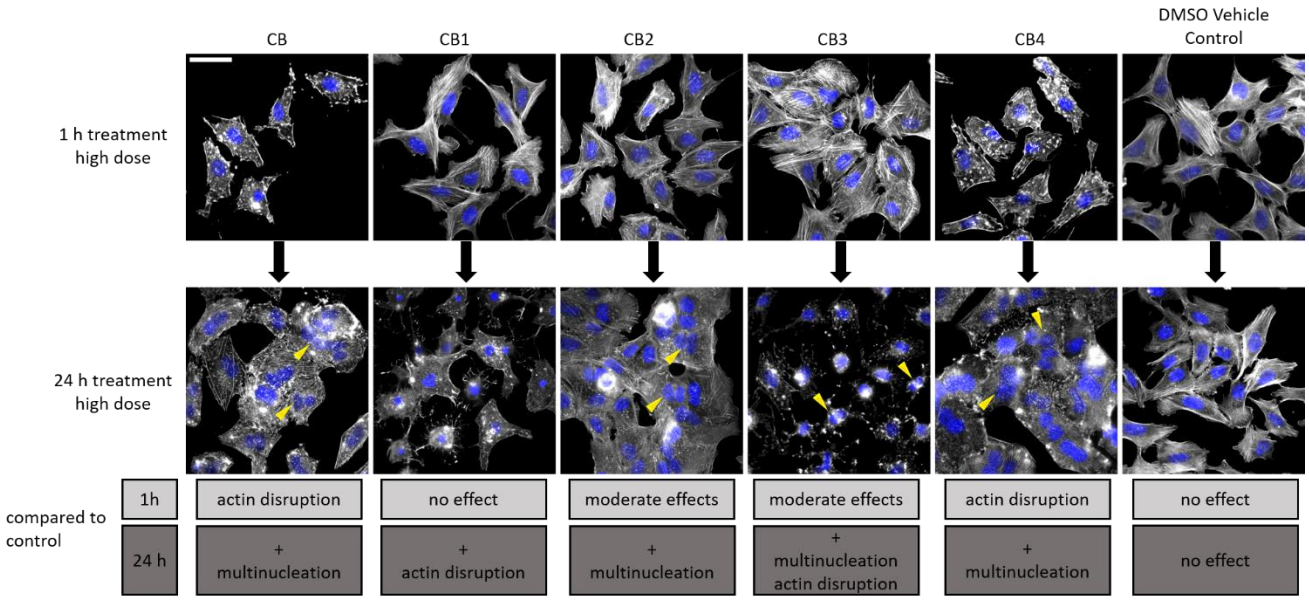

Figure 5 Long-term treatment of U-2OS cells with **CB** and **CB1** - **CB4** influences the degree of actin disruption and induces multinucleation. Cells were treated with high dose concentrations of indicated compounds for 1 h (upper row) and 24 h (lower row), fixed and stained for F-actin as described before. Multinucleated cells were marked with yellow arrowheads. Differences on actin and nuclei number of the cells between 1 h and 24 h treatment were summarized in grey boxes. Scale bar corresponds to 50 µm.

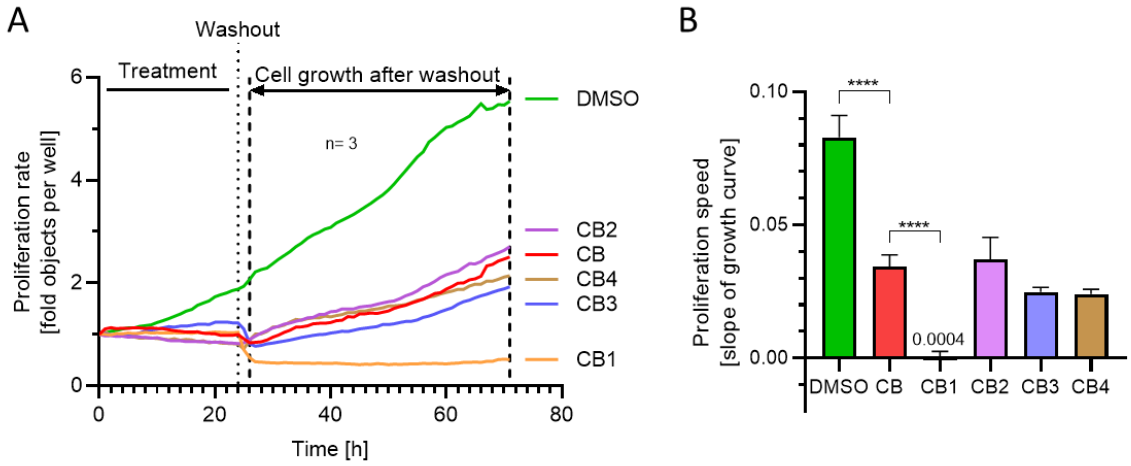

Figure 6 Analysis of cell proliferation during 24 h treatment followed by a 47 h regeneration phase. (A) Averaged growth curves of U-2OS cells during treatments as indicated. Proliferation rate was assessed by phase-contrast imaging and automated object counting for 71 h. The graph shows the means from at least three independent experiments with three replicates. (B) Proliferation speed during the recovery phase as determined by calculating the slopes from the growth curves between 26 and 71 hours (arrow). Data are means ± SD; n = 3. **** p<0.0001, ordinary one-way ANOVA.

We noticed massive changes in the amount of multinucleated cells and/or significant disruption of the actin network for the individual compounds. In case of **CB**, the most striking cellular alteration is the formation of multinucleated cells, which was already observed by Carter in 1967,[26] reminiscent of the outcome of **CB3** and **CB4** treatment (for clarification of the **CB3** effect on U-2OS cells after 24 h treatment, see Figure S1 in the Supplementary Information). Strikingly, the 24 h treatment with **CB1** evoked altered actin structures, however without inducing multinucleation, whereas **CB2** caused multinucleation, but left the actin network largely unchanged.

Next, we combined the 24 h treatment of U-2OS cells with a subsequent washout step and an additional recovery period of 47 h, to evaluate the ability of the affected actin network to regenerate (Figure 6). The number of cells stagnated during the treatment period with all the five compounds and dropped after the washout step, likely due the loss of detached and damaged cells. After washing, cells treated with **CB**, **CB2**-**CB4** slowly started to regenerate and proliferate, while recovery of **CB1**-treated cells was significantly diminished (Figure 6).

Staining procedures revealed a fully recovered actin network for **CB** and **CB2**-**CB4,** underlining the reversibility of this effect, whereas multinucleation was not fully overcome

after two days of recovery (See Figure S3 in the Supplementary Information). In contrast, cell proliferation was completely abolished upon treatment with **CB1**, although cells harbored a seemingly intact actin network. From this, we concluded that all compounds caused severe long-term effects on cell proliferation, even the 'non-toxic' **CB2**. Due to the strong effects upon long-term treatment with **CB1**, **CB3**, and **CB4**, we aimed to exclude the possibility that these compounds undergo conversion to **CB** by intracellular deacetylating enzymes, explaining increased activities. Hence, we attempted to re-extract the mentioned compounds from the medium after 24 h cell exposure. Indeed, we could detect an additional peak in the mass and UV spectra corresponding to **CB** when analyzing extracts derived from **CB3** and **CB4** treatment (See Figure S6 and S7 in the Supplementary Information), but not for **CB1**. This indicates that the acetyl groups in **CB3** and **CB4** can in fact be cleaved, potentially by e.g. histone deacetylases.[27] Notwithstanding this, no decomposition of **CB1** was observed (See Figure S5 in the Supplementary Information), so we assume that the cellular effects of **CB1** are inherent to the compound. The reduced actin disruption activity of C-7 *O*-acetylated cytochalasans has been described before,[4,28,29] whereas the antiproliferative, long-lasting cytostatic activity of **CB1** observed here deserves further investigations. For instance, **CB1** might interfere with actin-independent targets such as summarized by Lambert *et al.* (2023).[4] As known for decades, **CB** inhibits glucose transport in human erythrocytes with three existing binding sites (I-III) in the membrane.[30,31] Furthermore, it was shown that **CB1** (referred to as CB-7 monoacetate in reference 31) is able to bind site I of the glucose carrier and inhibits the glucose transport simultaneously.[31] Next to the glucose transport system, **CB** was described to display inhibitory activity on the human potassium channel hKv1.5[32], and it was hypothesized that C-7 acetylation in **CB1** lowered the cytotoxic activity by reduction of the ion channel activity rather than interfering with the actin cytoskeleton.[33] In addition, effects herein reported for **CB2** long-term treatment raise the pressing question whether pronounced multinucleation accompanied with a nearly unaffected actin network can be associated with hitherto unknown non-actin targets. Finally, we want to draw attention to the intracellular conversion of **CB3** and **CB4** that should be considered in the future regarding pharmacological application of cytochalasans in general and the interpretation of previous SAR studies on this natural product class.

The current study uncovers new evidence on the SAR of **CB** combining an *in silico* docking of **CB** onto actin, semi-synthesis of selected, delineated derivatives, and cell biological assays. In conclusion, the virtual docking of **CB** onto non-polymerizable actin revealed vital functional groups (i.e. NH group of the isoindolone core (N-2) and the hydroxyl groups at C-7) involved in stabilizing interactions with the amino acids of the active pocket of actin via hydrogen bonding. Furthermore, methylation at position N-2 and acetylation at the NH in positions N-2 and *O*-acetylation of the hydroxy function in C-7 and C-20 were carried out and afforded derivatives **CB1**, **CB2**, **CB3**, and **CB4**, respectively. All four compounds displayed a significant reduction of cytotoxicity in murine connective tissue fibroblasts L929, whereas compound **CB2** showed a complete loss of cytotoxicity. In line with this, short-term treatments revealed only mild effects on actin arrangements in the U-2OS cell model in case of **CB1**-**CB3**. *In vitro* actin polymerization assays supported that the respective affinity of these derivatives for actin itself is reduced. They also suggested that diminished cell permeability and thus availability to the actin cytoskeleton are not causative of the rather weak activity of modified compounds. In addition, the biological effects of **CB4**, bearing an acetylation at C-20, were virtually identical to those of **CB,** suggesting the C-20 OH group plays no crucial role in **CB**-actin interaction, which is perfectly in line with our initial docking results. Increased actin disruption by **CB3** upon prolonged treatments are likely caused by enzymatic deacetylation of the derivatives in the cytoplasm, converting them into the highly cytotoxic **CB**. Thus, we conclude that *N*-acetylation of *N*-2 is a poor candidate for pharmacological exploitation. In contrast, methylation of the same position gave the stable derivative **CB2**, displaying a moderate cytostatic activity in combination with a strongly reduced actin disruption activity, which deserves further scrutiny. Interestingly, acetylation of the hydroxy function at C-7 (derivative **CB1**) did not induce multinucleation. Instead, it completely blocked proliferation, despite its moderate effects on actin rearrangements. Whereas in principle, effects on mitosis and/or cytokinesis can be explained by inhibition of actin dynamics, the specific features of the four derivatives call for searching potential non-actin targets of these processes in the future. This particularly applies to **CB1**, the effects of which on actin is reversible, while proliferation remains blocked upon washout. Yet, our results confirm the importance of all but the C-20 hydroxyl function of the initially identified and chemically modified groups for **CB** potency in actin polymerization inhibition or F-actin disruption.

ASSOCIATED CONTENT

Data Availability Statement. The NMR data for **CB**, **CB1**, **CB2**, **CB3**, **CB4**, and **1**-**5** have been deposited at nmrXiv (https://nmrxiv.org) under the DOI: 10.57992/nmrxiv.p61.

Supporting Information. This material is available free of charge via the Internet at http://pubs.acs.org.
PDF file including experimental protocols for synthesis and biological evaluation, NMR spectra, HRMS spectra, and IR spectra.

AUTHOR INFORMATION

Corresponding Authors

Philipp Klahn Department of Chemistry and Molecular Biology, Division of Organic and Medicinal Chemistry, University of Gothenburg, Medicinaregatan 7B, SE-413 90 Göteborg, Sweden; https://orcid.org/0000-0003-4713-2345; E-mail: philipp.klahn@gu.se

Theresia Stradal Department of Cell Biology, Helmholtz Centre for Infection Research, Inhoffenstrasse 7, D-38124 Braunschweig, Germany; https://orcid.org/0000-0002-0352-9474 E-mail: theresia.stradal@helmholtz-hzi.de

Authors

Mervic D. Kagho Department of Chemistry and Molecular Biology, Division of Organic and Medicinal Chemistry, University

of Gothenburg, Medicinaregatan 7B, SE-413 90 Göteborg, Sweden; orcid.org/0000-0003-3714-7738.
Katharina Schmidt Department of Cell Biology, Helmholtz Centre for Infection Research, Inhoffenstrasse 7, D-38124 Braunschweig, Germany; orcid.org/0000-0003-1512-1748.
Christopher Lambert Department of Cell Biology, Department of Molecular Cell Biology, Department of Microbial Drugs, Helmholtz Centre for Infection Research, Inhoffenstrasse 7, D-38124 Braunschweig, Germany.
Thomas Kaufmann Institute for Biophysical Chemistry, Hannover Medical School, Carl-Neuberg Strasse 1, D-30625 Hannover, Germany.
Lili Jia Department of Microbial Drugs, Helmholtz Centre for Infection Research, Inhoffenstrasse 7, D-38124 Braunschweig, Germany.
Jan Faix Institute for Biophysical Chemistry, Hannover Medical School, Carl-Neuberg Strasse 1, D-30625 Hannover, Germany.
Klemens Rottner Department of Cell Biology, Department of Molecular Cell Biology, Helmholtz Centre for Infection Research, Inhoffenstrasse 7, D-38124 Braunschweig, Germany.
Marc Stadler Department of Microbial Drugs, Helmholtz Centre for Infection Research, Inhoffenstrasse 7, D-38124 Braunschweig, Germany; orcid.org/0000-0002-7284-8671.

Author Contributions

Contribution are given with CRediT definition according to Brand *et al.*[34]

Conceptualization: P.K. and T.S.; Methodology: M.D.K, K.S., T.K., P.K.; Software: P.K.; Validation: M.D.K. and K.S.; Formal analysis: M.D.K., K.S. and P.K.; Investigation: M.D.K., K.S., C.L., T.K., L.J. and P.K; Resources: P.K., T.S., K.R., M.S. and J.F; Data curation: P.K.; Writing—original draft: M.D.K., K.S., T.K., T.S. and P.K.; Writing—review & editing: all authors; Visualization: P.K., K.S. and M.D.K; Supervision: P.K., T.S., K.R., J.F. and M.S.; Project administration: M.D.K., K.S., P.K. and T.S.; Funding acquisition: P.K., T.S., M.D.K., K.R., M.S..

‡These authors contributed equally.

ACKNOWLEDGMENT

The authors thank Wera Collisi (HZI) for conduction of MIC and cytotoxicity assays. The authors thank the Swedish NMR Center (SNC, GU), the Proteomics Core Facility (PFC, GU) and the mass spectrometry and NMR spectroscopy units of the Institute of Organic Chemistry (TUBS) for analytical support. We gratefully acknowledge the German Research Foundation (DFG) for research funding through the CytoLabs consortium (DFG Research Unit FOR 5170) and an individual grant Fa330/12-3 to J.F.. M.D.K. is thankful to the German Academic Exchange Service (DAAD) for a Doctoral research grant (personal ref.no. 91693784). C.L. is grateful for a stipend granted by the Life Science Foundation (LSS, Munich). The content of this work is solely the responsibility of the authors and does not necessarily represent the official views of the funding agencies.

REFERENCES

The authors cite the following publications in the Supplementary Information.[10,12,38–42,17,18,22,23,25,35–37]

(1) Skellam, E. The Biosynthesis of Cytochalasans. *Nat. Prod. Rep.* **2017**, *34* (11), 1252–1263. https://doi.org/10.1039/C7NP00036G.
(2) Scherlach, K.; Boettger, D.; Remme, N.; Hertweck, C. The Chemistry and Biology of Cytochalasans. *Nat. Prod. Rep.* **2010**, *27* (6), 869–886. https://doi.org/10.1039/b903913a.
(3) Zhu, H.; Chen, C.; Tong, Q.; Zhou, Y.; Ye, Y.; Gu, L.; Zhang, Y. Progress in the Chemistry of Organic Natural Products. In *Progress in the Chemistry of Cytochalasans*; Kinghorn, A. D., Falk, H., Gibbons, S., Kobayashi, J., Asakawa, Y., Liu, J.-K., Eds.; Springer Cham, 2021; pp 1–134. https://doi.org/10.1007/978-3-030-59444-2_1.
(4) Lambert, C.; Schmidt, K.; Karger, M.; Stadler, M.; Stradal, T. E. B.; Rottner, K. Cytochalasans and Their Impact on Actin Filament Remodeling. *Biomolecules* **2023**, *13* (8), 1247. https://doi.org/10.3390/biom13081247.
(5) Rottner, K.; Faix, J.; Bogdan, S.; Linder, S.; Kerkhoff, E. Actin Assembly Mechanisms at a Glance. *J. Cell Sci.* **2017**, *130* (20), 3427–3435. https://doi.org/10.1242/jcs.206433.
(6) Pollard, T. D.; Craig, S. W. Mechanism of Actin Polymerization. *Trends Biochem. Sci.* **1982**, *7* (2), 55–58. https://doi.org/10.1016/0968-0004(82)90076-7.
(7) Lappalainen, P.; Kotila, T.; Jégou, A.; Romet-Lemonne, G. Biochemical and Mechanical Regulation of Actin Dynamics. *Nat. Rev. Mol. Cell Biol.* **2022**, *23* (12), 836–852. https://doi.org/10.1038/s41580-022-00508-4.
(8) Brown, S.; Spudich, J. Cytochalasin Inhibits the Rate of Elongation of Actin Filament Fragments. *J. Cell Biol.* **1979**, *83* (3), 657–662. https://doi.org/10.1083/jcb.83.3.657.
(9) Trendowski, M. Using Cytochalasins to Improve Current Chemotherapeutic Approaches. *Anticancer. Agents Med. Chem.* **2015**, *15* (3), 327–335. https://doi.org/10.2174/1871520614666141016164335.
(10) Nair, U. B.; Joel, P. B.; Wan, Q.; Lowey, S.; Rould, M. A.; Trybus, K. M. Crystal Structures of Monomeric Actin Bound to Cytochalasin D. *J. Mol. Biol.* **2008**, *384* (4), 848–864. https://doi.org/10.1016/j.jmb.2008.09.082.
(11) Joel, P. B.; Fagnant, P. M.; Trybus, K. M. Expression of a Nonpolymerizable Actin Mutant in Sf9 Cells. *Biochemistry* **2004**, *43* (36), 11554–11559. https://doi.org/10.1021/bi048899a.
(12) Friedrich, N.-O.; Flachsenberg, F.; Meyder, A.; Sommer, K.; Kirchmair, J.; Rarey, M. Conformator: A Novel Method for the Generation of Conformer Ensembles. *J. Chem. Inf. Model.* **2019**, *59* (2), 731–742. https://doi.org/10.1021/acs.jcim.8b00704.
(13) Rould, M. A.; Wan, Q.; Joel, P. B.; Lowey, S.; Trybus, K. M. Crystal Structures of Expressed Non-Polymerizable Monomeric Actin in the ADP and ATP States. *J. Biol. Chem.* **2006**, *281* (42), 31909–31919. https://doi.org/10.1074/jbc.M601973200.
(14) Oosterheert, W.; Blanc, F. E. C.; Roy, A.; Belyy, A.; Sanders, M. B.; Hofnagel, O.; Hummer, G.; Bieling, P.; Raunser, S. Molecular Mechanisms of Inorganic-Phosphate Release from the Core and Barbed End of Actin Filaments. *Nat. Struct. Mol. Biol.* **2023**, *30* (11), 1774–1785. https://doi.org/10.1038/s41594-023-01101-9.
(15) Carman, P. J.; Barrie, K. R.; Rebowski, G.; Dominguez, R. Structures of the Free and Capped Ends of the Actin Filament. *Science (80-.).* **2023**, *380* (6651), 1287–1292. https://doi.org/10.1126/science.adg6812.
(16) Binder, M.; Tamm, C.; Tuner, W. B.; Minato, H. Nomenclature of a Class of Biologically Active Mould Metabolites: The Cytochalasins, Phomins, and Zygosporins. *J. Chem. Soc . Perkin Trans. 1* **1973**, 1146–1147.
(17) Kretz, R.; Wendt, L.; Wongkanoun, S.; Luangsa-Ard, J. J.; Surup, F.; Helaly, S. E.; Noumeur, S. R.; Stadler, M.; Stradal, T. E. B. The Effect of Cytochalasans on the Actin Cytoskeleton of Eukaryotic Cells and Preliminary Structure–Activity Relationships. *Biomolecules* **2019**, *9* (2), 73. https://doi.org/10.3390/biom9020073.
(18) SeeSAR - MIDAS. BioSolveIT GmbH: Sankt Augustin, Germany 2023.
(19) Schneider, N.; Lange, G.; Hindle, S.; Klein, R.; Rarey, M. A Consistent Description of HYdrogen Bond and DEhydration Energies in Protein–Ligand Complexes: Methods behind the HYDE Scoring Function. *J. Comput. Aided. Mol. Des.* **2013**, *27* (1), 15–29. https://doi.org/10.1007/s10822-012-9626-2.
(20) Binder, M.; Tamm, C.; Turner, W. B.; Minato, H. Nomenclature of a Class of Biologically Active Mould Metabolites: The Cytochalasins, Phomins, and Zygosporins. *J. Chem. Soc. Perkin Trans. 1* **1973**, No. 1146, 1146–1147.

https://doi.org/10.1039/P19730001146.
(21) Zscherp, R.; Coetzee, J.; Vornweg, J.; Grunenberg, J.; Herrmann, J.; Müller, R.; Klahn, P. Biomimetic Enterobactin Analogue Mediates Iron-Uptake and Cargo Transport into E. Coli and P. Aeruginosa. *Chem. Sci.* **2021**, *12* (30), 10179–10190. https://doi.org/10.1039/D1SC02084F.
(22) Becker, K.; Wessel, A.-C. C.; Luangsa-Ard, J. J.; Stadler, M. Viridistratins A–C, Antimicrobial and Cytotoxic Benzo[j]Fluoranthenes from Stromata of Annulohypoxylon Viridistratum (Hypoxylaceae, Ascomycota). *Biomolecules* **2020**, *10* (5), 805. https://doi.org/10.3390/biom10050805.
(23) Kagho, M. D.; Hintersatz, H.; Ihle, A.; Zeng, H.; Schrey, H.; Colisi, W.; Klahn, P.; Stadler, M.; Bruhn, C.; Rüffer, T.; Lang, H.; Banert, K. Total Synthesis via Biomimetic Late-Stage Heterocyclization: Assignment of the Relative Configuration and Biological Evaluation of the Nitraria Alkaloid (±)-Nitrabirine. *J. Org. Chem.* **2021**, *86* (21), 14903–14914. https://doi.org/10.1021/acs.joc.1c01650.
(24) Cooper, J. A.; Walker, S. B.; Pollard, T. D. Pyrene Actin: Documentation of the Validity of a Sensitive Assay for Actin Polymerization. *J. Muscle Res. Cell Motil.* **1983**, *4* (2), 253–262. https://doi.org/10.1007/BF00712034.
(25) Breitsprecher, D.; Kiesewetter, A. K.; Linkner, J.; Faix, J. Analysis of Actin Assembly by in Vitro TIRF Microscopy. *Methods Mol. Biol.* **2009**, *571*, 401–415. https://doi.org/10.1007/978-1-60761-198-1_27.
(26) CARTER, S. B. Effects of Cytochalasins on Mammalian Cells. *Nature* **1967**, *213* (5073), 261–264. https://doi.org/10.1038/213261a0.
(27) Inoue, A.; Fujimoto, D. Histone Deacetylase from Calf Thymus. *Biochim. Biophys. Acta - Enzymol.* **1970**, *220* (2), 307–316. https://doi.org/10.1016/0005-2744(70)90015-X.
(28) Yahara, I.; Harada, F.; Sekita, S.; Yoshihira, K.; Natori, S. Correlation between Effects of 24 Different Cytochalasins on Cellular Structures and Cellular Events and Those on Actin in Vitro. *J. Cell Biol.* **1982**, *92* (1), 69–78. https://doi.org/10.1083/jcb.92.1.69.
(29) Matsumoto, M.; Minato, H.; Katayama, T.; Katagiri, K.; Matsuura, S.; Sunagawa, N.; Hori, K.; Harada, M.; Takeuchi, M. Structure-Activity Relationships among Zygosporin Derivatives. *Chem. Pharm. Bull.* **1973**, *21* (10), 2268–2277. https://doi.org/10.1248/cpb.21.2268.
(30) Bloch, R. Inhibition of Glucose Transport in the Human Erythrocyte by Cytochalasin B. *Biochemistry* **1973**, *12* (23), 4799–4801. https://doi.org/10.1021/bi00747a036.
(31) Rampal, A. L.; Pinkofsky, H. B.; Jung, C. Y. Structure of Cytochalasins and Cytochalasin B Binding Sites in Human Erythrocyte Membranes. *Biochemistry* **1980**, *19* (4), 679–683. https://doi.org/10.1021/bi00545a011.
(32) Choi, B. H.; Park, J.-A.; Kim, K.-R.; Lee, G.-I.; Lee, Y.-T.; Choe, H.; Ko, S.-H.; Kim, M.-H.; Seo, Y.-H.; Kwak, Y.-G. Direct Block of Cloned HKv1.5 Channel by Cytochalasins, Actin-Disrupting Agents. *Am. J. Physiol. Physiol.* **2005**, *289* (2), C425–C436. https://doi.org/10.1152/ajpcell.00450.2004.
(33) Van Goietsenoven, G.; Mathieu, V.; Andolfi, A.; Cimmino, A.; Lefranc, F.; Kiss, R.; Evidente, A. In Vitro Growth Inhibitory Effects of Cytochalasins and Derivatives in Cancer Cells. *Planta Med.* **2011**, *77* (07), 711–717. https://doi.org/10.1055/s-0030-1250523.
(34) Brand, A.; Allen, L.; Altman, M.; Hlava, M.; Scott, J. Beyond Authorship: Attribution, Contribution, Collaboration, and Credit. *Learn. Publ.* **2015**, *28* (2), 151–155. https://doi.org/10.1087/20150211.
(35) Branda, N. Liquids with Freeze-Pump-Thaw Cycling. *JoVE Science Education Database. Organic Chemistry.*; 2019.
(36) Still, W. C.; Kahn, M.; Mitra, A. Rapid Chromatographic Technique for Preparative Separations with Moderate Resolution. *J. Org. Chem.* **1978**, *43* (14), 2923–2925. https://doi.org/10.1021/jo00408a041.
(37) Mosmann, T. Rapid Colorimetric Assay for Cellular Growth and Survival: Application to Proliferation and Cytotoxicity Assays. *J. Immunol. Methods* **1983**, *65* (1–2), 55–63. https://doi.org/10.1016/0022-1759(83)90303-4.
(38) Wang, C.; Lambert, C.; Hauser, M.; Deuschmann, A.; Zeilinger, C.; Rottner, K.; Stradal, T. E. B.; Stadler, M.; Skellam, E. J.; Cox, R. J. Diversely Functionalised Cytochalasins through Mutasynthesis and Semi-Synthesis. *Chem. - A Eur. J.* **2020**, *26* (60), 13578–13583. https://doi.org/10.1002/chem.202002241.
(39) Doolittle, L. K.; Rosen, M. K.; Padrick, S. B. Measurement and Analysis of in Vitro Actin Polymerization. *Methods Mol. Biol.* **2013**, *1046*, 273–293. https://doi.org/10.1007/978-1-62703-538-5_16.
(40) Zscherp, R.; Chakrabarti, A.; Lehmann, A. P.; Schrey, H.; Zeng, H.; Collisi, W.; Klahn, P. Design of Non-Cytotoxic 6,7-Dihydroxycoumarin-5-Carboxylates with Antibiofilm Activity against Staphylococcus Aureus and Candida Albicans. *Org. Biomol. Chem.* **2023**, *21* (23), 4744–4749. https://doi.org/10.1039/D3OB00303E.
(41) Klahn, P.; Fetz, V.; Ritter, A.; Collisi, W.; Hinkelmann, B.; Arnold, T.; Tegge, W.; Rox, K.; Hüttel, S.; Mohr, K. I.; Wink, J.; Stadler, M.; Wissing, J.; Jänsch, L.; Brönstrup, M. The Nuclear Export Inhibitor Aminoratjadone Is a Potent Effector in Extracellular-Targeted Drug Conjugates. *Chem. Sci.* **2019**, *10* (20), 5197–5210. https://doi.org/10.1039/C8SC05542D.
(42) Reichenbach, H.; Höfle, G. Discovery and Development of the Epothilones : A Novel Class of Antineoplastic Drugs. *Drugs R. D.* **2008**, *9* (1), 1–10. https://doi.org/10.2165/00126839-200809010-00001.